AGU PUBLICATIONS

Geophysical Research Letters

RESEARCH LETTER
10.1002/2014GL062247

Key Point:
- Atmospheric moisture and convection have comparable effects on rainfall extremes

Supporting Information:
- Readme
- Text S1
- Text S2
- Figure S1
- Figure S2
- Figure S3

Correspondence to:
C. Lepore,
clepore@ldeo.columbia.edu

Citation:
Lepore, C., D. Veneziano, and A. Molini (2015), Temperature and CAPE dependence of rainfall extremes in the eastern United States, *Geophys. Res. Lett.*, *42*, doi:10.1002/2014GL062247.

Received 17 OCT 2014
Accepted 3 NOV 2014
Accepted article online 7 NOV 2014

Temperature and CAPE dependence of rainfall extremes in the eastern United States

Chiara Lepore[1], Daniele Veneziano[2], and Annalisa Molini[3,4]

[1]Lamont-Doherty Earth Observatory, Columbia University, Palisades, NY, USA, [2]Department of Civil and Environmental Engineering, MIT, Cambridge, Massachusetts, USA, [3]Institute Centre for Water Advanced Technology and Environmental Research (iWater), Masdar Institute of Science and Technology, Abu Dhabi, United Arab Emirates, [4]Department of Chemical and Environmental Engineering, Masdar Institute of Science and Technology, Abu Dhabi, United Arab Emirates

Abstract We analyze how extreme rainfall intensities in the Eastern United States depend on temperature T, dew point temperature T_d, and convective available potential energy CAPE, in addition to geographic sub-region, season, and averaging duration. When using data for the entire year, rainfall intensity has a quasi Clausius-Clapeyron (CC) dependence on T, with super-CC slope in a limited temperature range and a maximum around 25°C. While general, these features vary with averaging duration, season, the quantile of rainfall intensity, and to some extent geographic sub-region. By using T_d and CAPE as regressors, we separate the effects of temperature on rainfall extremes via increased atmospheric water content and via enhanced atmospheric convection. The two contributions have comparable magnitudes, pointing at the need to consider both T_d and atmospheric stability parameters when assessing the impact of climate change on rainfall extremes.

1. Introduction

The relationship between atmospheric temperature T and precipitation intensity I has been extensively investigated, mainly as a basis for predicting the effect of climate change on extreme rainfall. Some studies [*Allan and Soden*, 2008; *Held and Soden*, 2006; *O'Gorman*, 2012; *O'Gorman and Schneider*, 2009] use coarse-scale GCM projections under hypothetical future climate scenarios, while others [*Berg and Haerter*, 2011; *Berg et al*., 2009, 2013; *Haerter and Berg*, 2009; *Haerter et al*., 2010; *Lenderink and van Meijgaard*, 2008, 2009, 2010; *Lenderink et al*., 2011; *Utsumi et al*., 2011] analyze historical rainfall records and are often regional in scope.

Findings are usually compared to the Clausius-Clapeyron (CC) relation, which gives an about 7% $°C^{-1}$ increase of the water holding capacity of the atmosphere with temperature. Since precipitation feeds on atmospheric moisture, it is often argued that rainfall intensity should increase at about the CC rate, or possibly faster due to the additional effect of temperature on vertical fluxes [*Sugiyama and Shiogama*, 2010; *Trenberth*, 1999; *Trenberth*, 2011]. Several regional studies have observed super-CC rates over certain ranges of temperature. Some, using 5 min rainfall data [*Haerter and Berg*, 2009; *Berg et al*., 2013], attribute the super-CC rate to a shift in contribution from frontal to convective precipitation as temperature increases. Others [*Lenderink and van Meijgaard*, 2008, 2009, 2010; *Lenderink et al*., 2011; *Berg et al*., 2013] explain the super-CC rate through changes in the intensity of convection with temperature.

The relationship between log precipitation intensity and temperature ($\ln I - T$ relation from now on) varies geographically, with averaging duration d and rainfall percentile p. For example, using 5 min rainfall records from Germany, *Haerter et al*. [2010] obtain $\ln I - T$ slopes for different p, d, and temperature ranges. They find that at high temporal resolutions the $\ln I - T$ slope increases with increasing T and p, transitioning from CC to about 2CC value. The slope increase is less apparent at hourly or daily scales, possibly due to the effect of dry periods within those longer durations.

The trend of increasing rainfall intensity with temperature has been reported also in other studies in Europe [*Haerter et al*., 2010; *Lenderink and van Meijgaard*, 2008] but is not universal. In a global analysis of daily rainfall, *Utsumi et al*. [2011] categorize the $\ln I - T$ relationships as monotonically increasing, monotonically decreasing, or with a peak-like structure. They find in Europe a mostly monotonically increasing shape with super-CC slopes, whereas over much of the US the shape is peak-like and sub-CC. For Japan, they consider also hourly and sub-hourly resolutions, which confirm the peak-like structure found at the daily scale. The

authors suggest that the decrease above 25°C is due to the short duration of rainfall events at high temperatures. Another possible explanation is the relationship between dew point temperature T_d or relative humidity RH and temperature T. *Hardwick Jones et al*. [2010], *Lenderink et al*. [2011], and *Utsumi et al*. [2011 – supporting information] show that T_d or RH flattens or decreases for T above ~25°C. *Hardwick Jones et al*. [2010] interpret this as the cause of the peaked $\ln I - T$ curves in Australia. They further observe that in much of Australia the atmospheric moisture has oceanic origin and suggests that sea surface temperature and distance from the ocean control the location of the peak.

Mishra et al. [2012] explore the $\ln I - T$ relation in the conterminous US. However, their reported slopes, which are often super-CC, appear inconsistent with the findings of *Shaw et al*. [2011] as well as our own results. *Shaw et al*. [2011] also find that the slopes vary considerably with region and season.

While it is generally recognized that rainfall intensity is controlled not just by available moisture but also by atmospheric convection, we are unaware of systematic investigations of how atmospheric stability parameters like the convective available potential energy CAPE affect rainfall extremes.

CAPE is an energy-based measure of atmospheric stability, which controls the maximum velocity that a positively buoyant air parcel can acquire through adiabatic ascent [*North and Erukhimova*, 2009]. It is used in the analysis and forecast of severe weather and rainfall [*Brooks et al*., 2003; *Markowski et al*., 2002], cumulus parameterization [*Ye et al*., 2010], and the characterization of convective precipitation [*Alfieri et al*., 2008; *Wallace*, 1975]. Under idealized conditions, if a fixed fraction of CAPE is transformed into kinetic energy, the vertical velocity of an ascending air parcel and hence the condensation rate and the intensity of rainfall, are proportional to $\sqrt{CAPE}$ [*Bluestein*, 1993, p. 444; *North and Erukhimova*, 2009, pp. 181–186]. While this argument ignores vertical wind shear, entrainment, and other factors, one might still anticipate a log-linear relationship between rainfall intensity and CAPE.

Here we investigate the relationship between intense precipitation and T, T_d and CAPE using records from the US east of the Rockies (EUS). We focus on the regression of the log-quantiles $\ln I_p$ against these variables and their dependence on geographic location, season, and rainfall averaging duration. By jointly regressing $\ln I_p$ against T_d and $\ln CAPE$, we separate two main pathways of temperature influence on extreme rainfalls: moisture availability and the enhancement of atmospheric convection. We also assess the efficiency of these two mechanisms in affecting intense precipitation.

2. Data

We obtained the hourly precipitation time series from the National Climatic Data Center (NCDC). Of the approximately 6000 NCDC stations, 270 CONUS (Conterminous United States) records were retained. These records do not include long data gaps, have few missing values, and are free of hourly estimates from disaggregated daily totals. They have data since 1979 and therefore overlap the ERA records (see below). Of the 270 stations, 182 are in the EUS region we study.

Mean daily air temperatures T were extracted from the sub-daily screen level (2 m) temperatures of ERA-Interim—the most recent reanalysis product of the European Center for Medium Range Weather Forecasts (ECMWF) [*Dee et al*., 2011]. ERA 12 h predicted fields were used to derive daily average CAPE estimates from the 00 and 12UTC samples. These data span the period 1979–2008 and were bi-linearly interpolated to a spatial resolution of 0.125 from the original 0.75° reduced Gaussian grid [*Berrisford et al*., 2009; for details on how CAPE is calculated, see *European Centre for Medium-Range Weather Forecast* (*ECMWF*), 2013]. Daily time series of T and CAPE for the NCDC stations were taken from the closest interpolated reanalysis cell.

To determine spatial gradients, we partition the EUS into four sub-regions (*North*, *Central*, *East* and *South*, as shown in Figure 1) and pool the data within each region. This produces much larger sample sizes and more stable results for the high-quantile analysis.

For 49 of the EUS stations we also obtain dew point temperature (T_d) from the NCDC Integrated Global Radiosonde Archive [IGRA, *Durre et al*., 2006] and infer daily average T_d values from bi-daily radio-soundings (00 and 12UTC) at the m.s.l. For completeness, we consider also the use of CAPE values from soundings (data and documentation available at http://www.ncdc.noaa.gov/oa/climate/igra/). The radiosonde stations are matched to the nearest NCDC gauge station and grouped by sub-region in analogy with the other variables.

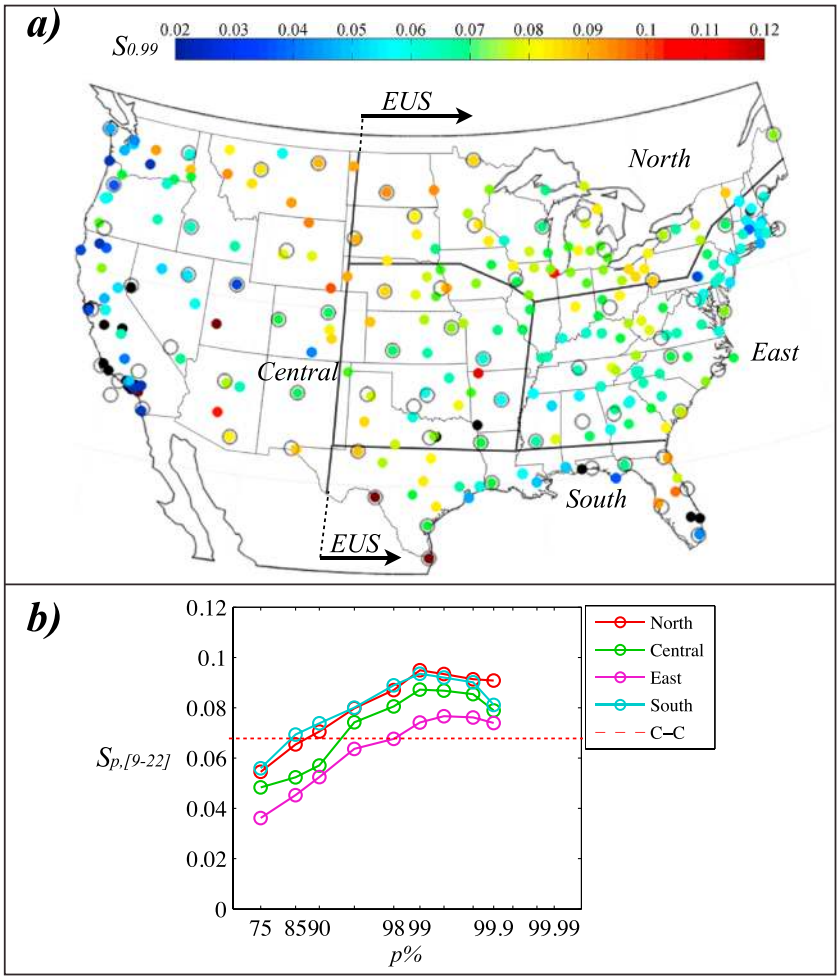

Figure 1. (a) Slope $S_{0.99}$ for the 270 Conterminous United States (CONUS) National Climatic Data Center (NCDC) stations (colored circles) and location of the 73 radiosonde stations (empty black circles). (b) $S_{p,[9-22]}$ as a function of p for the four sub-regions. The horizontal red line indicates the CC rate.

3. Methods

After matching the Precipitation Intensity (I) and Temperature (T) data series, we bin I into 2° temperature intervals 0–2, 2–4, …°C (we consider only positive temperatures). For each resulting time series I_T, we extract precipitation quantiles for several non-exceedance probabilities p, resulting in a matrix of rainfall intensities $I_{p,T}$.

The dependence of rainfall intensity on T is displayed through *quantile plots*, which are plots of $I_{p,T}$ against T for different p. Through regression of $\ln I_{p,T}$ against T, we infer, for each p, different measures of sensitivity of $\ln I_p$ to temperature: the overall slope S_p based on all available temperature bins, the average slope $S_{p,[T_1,T_2]}$ within a selected range of temperatures $[T_1, T_2]$, and the local slope $S_{p,T} = \frac{\partial \ln I_{p,T}}{\partial T}$. The local slope is estimated through locally-weighted linear regression, using a Gaussian kernel along temperature and a linear weighting scheme with maximum weight for the p-quantile of interest and lower weights for the two closest quantiles. We refer to plots of $S_{p,T}$ against T for given p as *slope-plots*.

Under the CC assumption, rainfall intensity has simple scaling with temperature, and the slope plots are parallel straight lines with approximate slope $\ln(1.07) = 0.068$ [*Lawrence*, 2005], but in reality $S_{p,T}$ has a more complex behavior, as discussed below.

The same methods are applied to T_d and CAPE, to generate I_{p,T_d} and $I_{p,CAPE}$ matrices and corresponding quantile and slope plots.

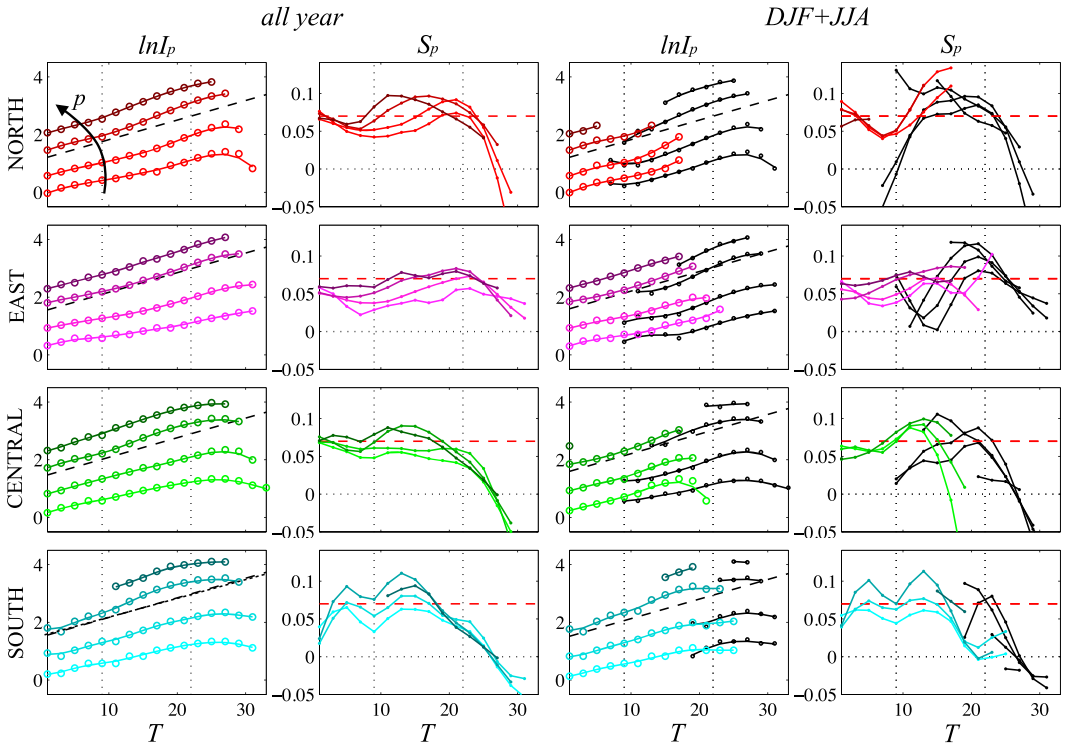

Figure 2. Quantile and slope plots for the four sub-regions for different probabilities levels. The dotted vertical lines mark 9 and 22°C, while the black dashed lines (first and third column) and red dashed lines (second and fourth column) show the CC rate. First two columns are for the all-year analysis. The last two columns are for winter (December, January, and February (DJF), colored lines) and summer (June, July, and August (JJA), black lines).

4. Results and Discussion

4.1. Dependence of Hourly Rainfall Extremes on Temperature T

Figure 1a shows the 270 NCDC stations (colored circles) and 73 radiosonde stations (empty black circles) in the conterminous US.

The colors of the circles give the slope $S_{0.99}$ calculated for the whole year. Black dots are for negative slopes, which are found occasionally in the North-East and more prevalently along the Pacific Coast. Along the eastern seaboard, the slopes tend to increase southward, but Florida includes a mix of high and low values, possibly due to the southward transition from humid subtropical climate to equatorial climate. Values in the Midwest region are close to the CC slope, fluctuating between 5 and 8%. The Rockies and the West, which are not included in the second part of the analysis, display a high and unique variability, due to the interplay of aridity, topography, and different moisture sources. In the following analysis we focus on the 182 NCDC and 49 radiosonde stations inside the EUS region.

Figure 1b shows plots of the slope $S_{p,[9-22]}$ against p, using data aggregated by region, in the temperature range [9–22°C] (the reason for this choice of temperature range is given below). The slope increases with increasing quantile, transitioning from sub-CC to super-CC for p around 0.9–0.99 depending on region. This trend is consistent with much of the literature [for example *O'Gorman*, 2012]. Seasonal results (not shown) are generally similar, although with somewhat different average slopes.

Figure 2 shows quantile and slope plots, $\ln I_p$ vs. T and S_p vs. T, respectively, for the whole year (first two columns) and winter (December, January, and February (DJF)) and summer (June, July, and August (JJA)) superposed (last two columns—colored for winter, black for summer). Results for the spring and fall seasons are close to the all-year results and are omitted. The four curves in each panel correspond to $p = 0.75, 0.9, 0.99$, and 0.999, with darker color tones for larger p. In the quantile plots, the circles are empirical values (they are missing when the data include fewer than 10 values above the quantile) and the lines are obtained

through locally weighted regression, as explained above. The same regression is used to estimate the local slopes. The vertical dotted lines delimit the 9–22°C temperature range, inside which the quantile curves are nearly straight; this is the range used to obtain $S_{p,[9-22]}$ in Figure 1b. The black dashed lines in the quantile plots and the red dashed lines in the slope plots show the CC slope. Most of the super-CC slopes are within the 9–22 temperature range, but even the maximum local slopes remain below 1.5CC except for isolated seasonal cases involving high quantiles. Other interesting features of Figure 2 are:

1. The slopes for the whole year have a local minimum around 8–10°C. This feature is amplified in the winter;
2. The slope plots for the winter (after the initial local minimum) and the summer have a "parabolic" shape. The "zeros" of the parabola, which for example occur at about $T = 10$ and 25°C in the North during the summer, correspond to local minima and maxima of the quantile plots. The peak of the parabola, approximately midway between the zeros, is the temperature at which I_p is most sensitive to T. This temperature tends to decrease as p increases. The winter and summer peaks are separated by about 10°C in the East and Central regions, but by a smaller amount in the South where the climate has less seasonality. The same is true for the "higher zeros", which correspond to the peaks of I_p; see for example the seasonal shift of the peaks in the Central and South regions.
3. The parabolic shape of the slope curves corresponds to an "S" shape of the quantile plots. This is clearest in the summer for the East, Central, and North regions (in the South there is an insufficient range of summer temperatures to fully observe the S-shape).
4. In all regions, the summer slopes decrease sharply above about 22°C.

The annual plots are the superposition of seasonal contributions. For example, the local peaks in the annual slope plots are generally contributed by different seasons. Pooling the data for the whole year obviously makes the seasonal features less visible, except for the summer, which is the only season when very high temperatures occur.

The temperature of the peak rainfall intensity, T_{max}, depends on season: in the summer, T_{max} is around 25°C. To explain the peaked shape of the quantile plots, we analyze both hypotheses brought forth in the literature: the moisture-limited hypothesis (the dew point temperature T_d declines above the temperature T_{max} of the peak), and the resolution-limited hypothesis (rainstorm duration is often sub-hourly for $T > T_{max}$).

Figure S1 (in the supporting information) shows that at high temperatures during the summer the average storm duration is short, supporting the resolution-limited hypothesis. However, in the Central and South regions in winter, T_{max} is around 18°C, and the average storm duration at that temperature is approximately 6 h. These features persist if one considers only the more intense storms (not shown). Therefore the resolution-limited hypothesis does not explain all the seasonal peaks.

The supporting information (Text S1) includes the $(\ln I - T)$ relation for averaging durations $d = 2$, 8 h and for daily averages and compares results for d intervals inside storms with those from block averaging. Consistently with *Haerter et al.* [2010], the slopes decrease with increasing d, especially for block averaging, most likely due to the higher dry fraction.

The moisture-limited hypothesis is examined in the following section, where we consider the dependence of rainfall intensity on T_d.

4.2. Dependence of Hourly Rainfall Extremes on Dew Point Temperature T_d

Next we investigate the dependence of the quantiles T_{dp} of T_d on temperature T and the dependence of the rainfall quantiles I_p on T_d. Matrices $T_{dp,T}$ and I_{p,T_d} are obtained for each 2° T interval (here both T and T_d are from sounding stations) and then used to produce quantile and slope plots similar to those in Figure 2. As *Hardwick Jones et al.* [2010] and *Lenderink et al.* [2011] observe, a peak-like T_d-T relationship would support the moisture-limited hypothesis for the peaked shape of the $\ln I_p$-T plots.

Figure 3a shows results for the Central and East regions (for the North and South regions, see Figure S2). Columns 1 and 3 show quantile plots of T_d against T for $p = 0.25$, 0.5, 0.75, and 0.99 for all-year (column 1) and winter + summer superposed (Column 3, summer in black). Columns 2 and 4 show quantile plots of $\ln I_p$ against T_d.

For the whole year, the T_d quantiles have a nearly 1:1 slope with T up to about 22°C and then decline. In coastal regions (East and South) the inflection point is at higher temperatures, and the spread $\Delta T = T - T_d$ is

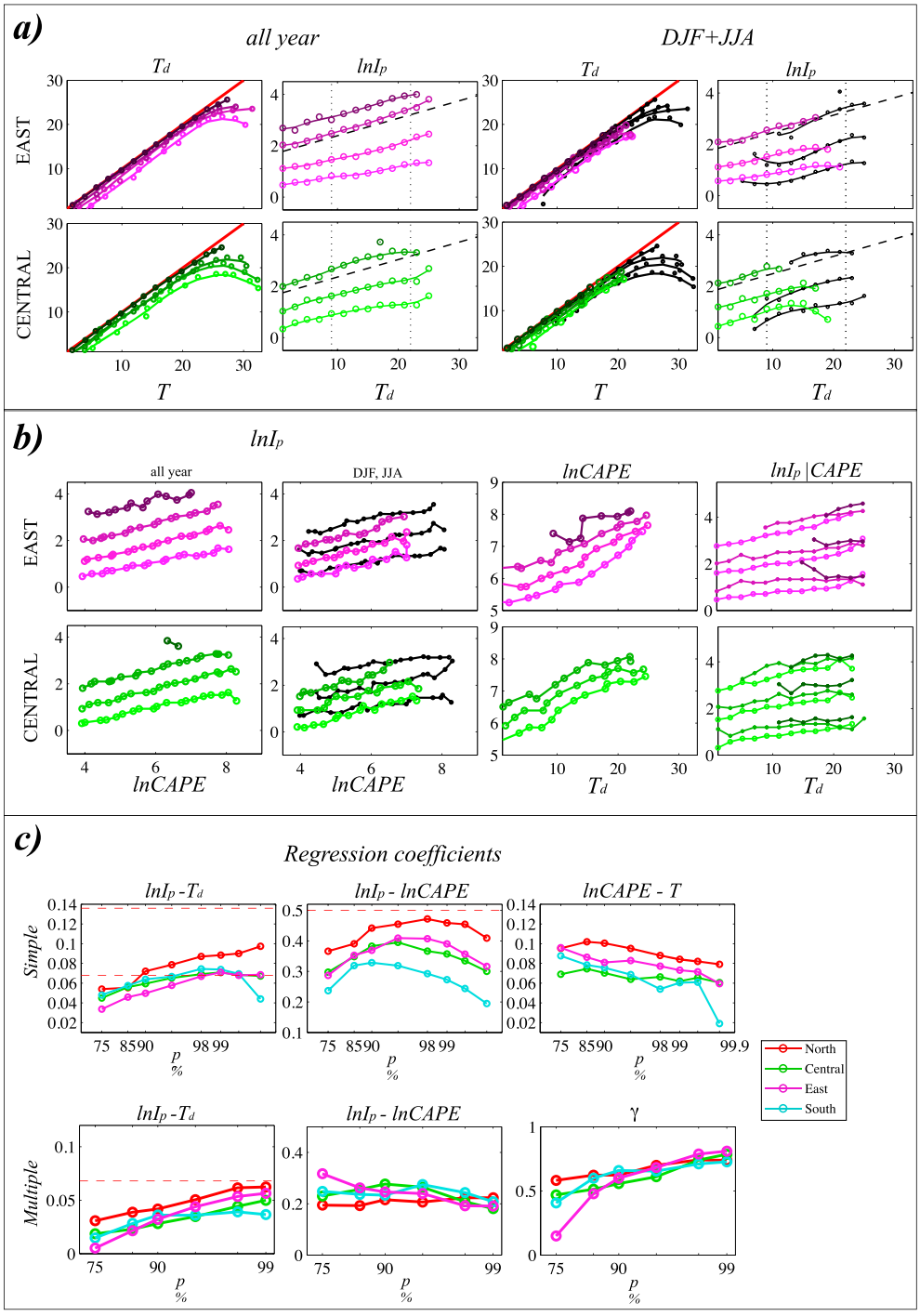

Figure 3. (a) $T_d - T$ and $\ln I - T_d$ quantile plots for all-year (first and second columns) and DJF and JJA superposed (colored and black lines, respectively, third and fourth columns). (b) $\ln I - \ln CAPE$ plots for all-year (first column) and DJF + JJA (second column). The third column shows $\ln CAPE - T_d$ quantiles, and the last column shows $\ln I - T_d$ relationships for different CAPE classes (see Results section for details). (c) Slope coefficients of simple $\ln I - T_d$, $\ln I - \ln CAPE$, and $\ln CAPE - T$ regressions (first row), and for multiple regression (equation (2)), and γ (second row; see text for details).

smaller than in inland regions (North and Central). This is consistent with the observations by *Hardwick Jones et al.* [2010] on the influence of sea surface temperature and proximity to the ocean. Column 3 shows that during the winter there is a similar inflection in the East region around 18°C, whereas in the Central region the winter inflection is less visible.

The quantile plots of I_p against T_d in Columns 2 and 4 are similar to those against T in Figure 2 (same quantiles are plotted), but they are straighter especially when data for the entire year are used. Hence, the fact that relative humidity decreases at very high temperatures explains at least in part the peaked shape of the quantile plots in Figure 2.

Shaw et al. [2011] suggest that daily T values are not representative of temperature at the time of precipitation. To understand whether the simultaneity of the measurements and differences in the temporal resolution pose significant issues, we have repeated analyses (*a*) and (*b*) with only rainfall data lagging the sounding measurements by at most 4 h. We have found no significant difference. Therefore, the lack of simultaneity does not have a large effect on T and T_d.

4.3. Dependence of Hourly Rainfall Extremes on CAPE and Joint Dependence on T_d and CAPE

To understand the role of atmospheric convection on extreme rainfall, we repeat the rainfall quantile analysis using ln(*CAPE*) as regressor, either by itself or in conjunction with T_d. In the latter case, based on the CC relationship and idealized parcel theory, one would expect a dependence of the type [*North and Erukhimova*, 2009]

$$\ln I_p = c + 0.058 T_d + 0.5 \ln CAPE \tag{1}$$

where c is a constant. Equation (1) assumes that rainfall intensity is proportional to the atmospheric moisture content near the ground and that a fixed fraction of CAPE is converted to updraft velocity. In reality, the slope coefficients may deviate from 0.068 and 0.5 due to entrainment, vertical wind shear, and other factors.

The first two columns of Figure 3b show plots of $\ln I_p$ against $\ln CAPE$, for the whole year (first column) and winter-summer superposed (second column). Regions and quantiles are the same as in Figures 3a and 2. The plots are remarkably straight and parallel, indicating that rainfall intensity has a simple-scaling relationship with CAPE. Specifically, the rainfall quantiles I_p vary in approximation as $CAPE^{\beta}$, where β depends on region and season (the range is 0.2–0.4, with largest values for winter in the North and smallest values for summer in the South), but is insensitive to p. The third column of Figure 3b shows plots of the quantiles $\ln CAPE$ against T_d. As expected, $\ln CAPE$ and T_d have a positive correlation.

To separate the contributions made by T_d and $\ln CAPE$ to the rainfall intensity quantiles, we classify the rainfall intensity data into discrete cells on the (T_d, $\ln CAPE$)-plane, and for each cell estimate the rainfall quantiles $I_{p|T_d,\ln CAPE}$. The last column of Figure 3b shows plots of the raw estimates of $\ln I_{p|T_d,\ln CAPE}$ against T_d for three classes of CAPE ($<$500, [500–1500], and $>$1500 J/kg) and three values of p (0.75, 0.9, and 0.99). Darker color tones identify higher CAPE values. To avoid overlapping, the values for $p = 0.9$ are translated upwards by 0.5 and those for $p = 0.99$ are translated by 1.0. The rainfall quantiles I_p increase as either T_d or $\ln CAPE$ increases. While there is some interaction between the two regressors (the slope of $\ln I_p$-T_d decreases as $\ln CAPE$ increases), for ease of interpretation we have fitted a regression model without interaction, of the type

$$\ln I_p = c + \alpha T_d + \beta \ln CAPE \tag{2}$$

with parameters c, α, and β. Equation (2) has the same structure as equation (1) but allows the slope parameters to differ from their ideal theoretical values.

The slopes of several fitted regressions are displayed in Figure 3c. The top row gives, from left to right, the slopes of simple linear regressions of $\ln I_p$ against T_d, $\ln I_p$ against $\ln CAPE$, and $\ln CAPE$ against T. The plots in the second row give the slopes α and β in equation (2). It is interesting that, on average, α and β are about one half the "theoretical" values in equation (1) (this is due to neglected phenomena like entrainment and vertical wind shear). While α increases significantly as p increases, β is essentially constant with p. The low values of α and β relative to equation (1) indicate that the efficiency with which water vapor is converted to rainfall and the CAPE potential energy is converted to kinetic energy is lower when water vapor and CAPE are higher (and when temperature T is higher). This lower conversion efficiency is reflected in the sub-CC slopes of the low rainfall quantiles.

One can use the estimates of α and β and the slopes δ of the regressions of $\ln CAPE$ against T to evaluate the relative contribution of T_d (water vapor content) and $\ln CAPE$ (intensity of convection) on the slope of the quantile plots $\ln I_p$-T. Since the regression of T_d against T has nearly unitary slope, the relative contribution of

T_d can be found as $\gamma = \frac{\alpha}{\alpha+\delta\beta}$. The panel at the bottom of Figure 3c shows γ as a function of the non-exceedance probability p. The values are highly consistent across regions and vary from about 0.5 for $p = 0.75$ (meaning equal contribution from variation with T of water vapor content and the intensity of convection) to about 0.8 for $p = 0.99$ (predominance of water vapor variation).

4.4. Sounding Measurements and ERA Interim Values

The $\ln I_p$ -T results presented in sections 4*a* and 4*b* are based on different data sets (ERA vs. sounding) but are virtually identical. This is likely due to the fact that the ERA Interim fields assimilate a variety of quality-checked observations (ground measurements, atmospheric soundings, and remotely sensed fields) through space-time consistent procedures (4D variational assimilation; see *Dee et al.* [2011]).

Given the extreme fine-scale variability of CAPE and precipitation, it is a priori not clear what time-space scale of CAPE is best to predict intense rainfall [*Thompson et al*., 2003]. For example, there is evidence that correlation between CAPE from soundings and simultaneous rainfall is significant when precipitation is dominated by local surface forcing, but not in other cases [*Adams and Souza*, 2009]. For completeness, we have compared the results from using CAPE from ERA Interim (*CAPErean*) as done above and from soundings (*CAPEsound*, data and documentation available at http://www.ncdc.noaa.gov/oa/climate/igra/). When *CAPEsound* is used, the imposition of strict simultaneity with the rainfall measurements results in too small samples; hence, we have retained all rainfall measurements within 3 h windows centered on the soundings.

The main effect of using *CAPEsound* is a decrease in the $\ln I_p$-ln*CAPE* slope and an increase of γ toward 1, suggesting a weaker dependence of rainfall on the potential intensity of convection (see Text S2 for details). This result may be linked to the limited explanatory power of instantaneous CAPE measurements on extreme rainfall.

5. Conclusions

Our main findings can be summarized as follows:

1. We have evaluated the rainfall intensity-temperature ($\ln I - T$) relation in the EUS using ground observations, soundings, and reanalysis products. Our focus is on rainfall intensity quantiles I_p with $p \geq 0.75$. Within the EUS, the variation in the $\ln I_p$ -T relationships is relatively small, except in winter. The differences between the EUS and the western part of the country are much sharper.
2. We compared global and local slopes of the $\ln I_p$ -T relationships to the C-C rate. The overall range of these slopes is in line with prior literature for the EUS [*Shaw et al*., 2011; *Utsumi et al*., 2011]. This includes the "peak-like structure" with maximum rainfall intensity at about 22°C. However, contrary to *Mishra et al*. [2012], we rarely see super-CC rates. Such rates occur almost exclusively in an intermediate range of temperatures and only for the highest quantiles and rarely exceed 150% of the CC value.
3. We separated the two main pathways through which temperature affects precipitation (increased water vapor and enhanced atmospheric convection) by jointly regressing $\ln I_p$ against dew point temperature T_d and CAPE; see equation (2). We found that, given T_d, there is a power law relationship between rainfall intensity quantiles and CAPE, $I_p \propto CAPE^{\beta}$, with $\beta \approx 0.2 - 0.4$ depending on region. These exponents are much below the value 0.5 if a fixed fraction of CAPE was converted to kinetic energy. Hence, the energy-conversion mechanism is less efficient when CAPE is higher.
4. By contrast, the dependence of I_p on T_d for given CAPE varies significantly with p (see lower left panel of Figure 3c): for $p = 0.75$ the ($\ln I_p - T_d$) slope is around 0.02 (much lower that the CC value 0.068), whereas for the high quantiles the slope is about 80% of CC. Therefore, also the mechanism of converting atmospheric moisture to rainfall is inefficient, with a smaller converted fraction as atmospheric moisture increases.
5. We investigated the peak-like structure of the ($\ln I_p - T$) curves to determine whether the temperature $T_{\max}$ at the peak varies seasonally and regionally (it does) and whether the peak is due to a limit in the amount of moisture in the atmosphere or to the fact that at higher temperatures a larger fraction of rainstorms have sub-hourly duration (the primary cause is the limit on T_d). Therefore, to quantify extreme rainfall under possible future warmer climates it is important to assess the seasonal and annual limits of T_d. It is also important to quantify how CAPE will change, although CAPE is more influential on the lower quantiles of rainfall intensity.

Limitations and future extensions:

1. We used data from diverse sources (NCDC for *I*, *CAPE* from the assimilated and modeled fields of ERA and *T* and T_d from IGRA) and with different spatiotemporal resolution. It would be desirable to validate our results using a more uniform data set;
2. Understanding the root causes of the inefficiencies of the moisture-rainfall and potential-to-kinetic energy conversions and consideration of frontal versus convective precipitation could help explain the regional and seasonal patterns of rainfall intensity with temperature;
3. Differences were found when using CAPE values from soundings instead of ERA Interim estimates, suggesting the need to make a more detailed analysis of CAPE-related indices.
4. Finally, other atmospheric parameters could be included. We made an attempt in this direction by considering the total column water vapor and the dew point depression $T - T_d$, but found that these variables have negligible additional explanatory power on rainfall intensity, once T_d and CAPE are included.

Acknowledgments

All data used in this manuscript are available directly from online repositories listed in the Section on Data. They can also be obtained directly from the authors of this manuscript. C. Lepore and D. Veneziano acknowledge funding from the National Science Foundation under Grant EAR-0910721. A. Molini was funded by the Masdar Institute (One-to-One MIT-MI, 12WAMA1 and Flagship 12WAMC1) in the framework of the MIT and Masdar Institute Cooperative Program. Chiara Lepore acknowledges support from Lamont Doherty Earth Observatory and Columbia Department of Earth and Environmental Sciences. We are grateful to Tanvir Ahmed and Seonkyoo Yoon for the processing and quality control of the NOAA data. We thank three anonymous reviewers for their valuable feedback.

M. Bayani Cardenas thanks three anonymous reviewers for their assistance in evaluating this paper.

References

Adams, D. K., and E. P. Souza (2009), CAPE and Convective Events in the Southwest during the North American Monsoon, *Mon. Weather Rev.*, *137*(1), 83–98, doi:10.1175/2008MWR2502.1.

Alfieri, L., P. Claps, and P. D'Odorico (2008), An analysis of the soil moisture feedback on convective and stratiform precipitation, *J. Hydrometeorol.*, *9*, 280–291, doi:10.1175/2007JHM863.1.

Allan, R. P., and B. J. Soden (2008), Atmospheric warming and the amplification of precipitation extremes, *Science*, *321*, 1481–1484.

Berg, P., and J. O. Haerter (2011), Unexpected increase in precipitation intensity with temperature—A result of mixing of precipitation types?, *Atmos. Res.*, doi:10.1016/j.atmosres.2011.05.012.

Berg, P., J. O. Haerter, P. Thejll, C. Piani, S. Hagemann, and J. H. Christensen (2009), Seasonal characteristics of the relationship between daily precipitation intensity and surface temperature, *J. Geophys. Res.*, *114*, D18102, doi:10.1029/2009JD012008.

Berg, P., C. Moseley, and J. O. Haerter (2013), Strong increase in convective precipitation in response to higher temperatures, *Nat. Geosci.*, doi:10.1028/NGEO1731.

Berrisford, P., D. Dee, K. Fielding, and M. Fuentes (2009), The ERA-Interim Archive, *ECMWF Rep. Ser.* (ERA Report Series.), Shinfield Park, Reading, U. K.

Bluestein, H. B. (1993), *Synoptic-Dynamic Meteorology in Middle Latitudes*, II Observations and Theory of Weather Systems, 594 pp., Oxford Univ. Press, New York.

Brooks, H. E., J. W. Lee, and J. P. Craven (2003), The spatial distribution of severe thunderstorm and tornado environments from global reanalysis data, *Atmos. Res.*, *67-68*, 73–94, doi:10.1016/S0169-8095(03)00045-0.

Dee, D. P., et al. (2011), The ERA-Interim reanalysis: Configuration and performance of the data assimilation system, *Q. J. R. Meteorol. Soc.*, *137*(656), 553–597, doi:10.1002/qj.828.

Durre, I., R. S. Vose, and D. B. Wuertz (2006), Overview of the Integrated Global Radiosonde Archive, *J. Clim.*, *19*, 53–68.

European Centre for Medium-Range Weather Forecast (ECMWF) (2013), *IFS DOCUMENTATION*, 40 ed., ECMWF, Shinfield Park, Reading, RG2 9AX, England.

Haerter, J. O., and P. Berg (2009), Unexpected rise in extreme precipitation caused by a shift in rain type?, *Nat. Geosci.*, *2*(6), 372–373.

Haerter, J. O., P. Berg, and S. Hagemann (2010), Heavy rain intensity distributions on varying time scales and at different temperatures, *J. Geophys. Res.*, *115*, D17102, doi:10.1029/2009JD013384.

Hardwick Jones, R., S. Westra, and A. Sharma (2010), Observed relationships between extreme sub-daily precipitation, surface temperature, and relative humidity, *Geophys. Res. Lett.*, *37*, L22805, doi:10.1029/2010GL045081.

Held, I. P., and B. J. Soden (2006), Robust responses of the hydrological cycle to global warming, *J. Clim.*, *19*, 5686–5699.

Lawrence, M. G. (2005), The relationship between relative humidity and the dewpoint temperature in moist air: A simple conversion and applications, *Bull. Am. Meteorol. Soc.*, *86*, 225–233, doi:10.1175/BAMS-86-2-225.

Lenderink, G., and E. Van Meijgaard (2008), Increase in hourly precipitation extremes beyond expectations from temperature changes, *Nat. Geosci.*, *1*(8), 511–514.

Lenderink, G., and E. van Meijgaard (2009), Unexpected rise in extreme precipitation caused by a shift in rain type?, *Nat. Geosci.*, *2*(6), 373–373.

Lenderink, G., and E. van Meijgaard (2010), Linking increases in hourly precipitation extremes to atmospheric temperature and moisture changes, *Environ. Res. Lett.*, *5*, 025208, doi:10.1088/1748-9326/5/2/025208.

Lenderink, G., H. Y. Mok, T. C. Lee, and G. J. V. Oldenborgh (2011), Scaling and trends of hourly precipitation extremes in two different climate zones – Hong Kong and Netherlands, *Hydrol. Earth Syst. Sci.*, *15*(9), 3033–3041, doi:10.5194/hess-15-3033-2011.

Markowski, P. M., J. M. Straka, and E. N. Rasmussen (2002), Direct surface thermodynamic observations within rearflank downdrafts of nontornadic and tornadic supercells, *Mon. Weather Rev.*, *130*, 1692–1721.

Mishra, V., J. M. Wallace, and D. P. Lettenmaier (2012), Relationship between hourly extreme precipitation and local air temperature in the United States, *Geophys. Res. Lett.*, *39*, L16403, doi:10.1029/2012GL052790.

North, G. R., and T. L. Erukhimova (2009), *Atmospheric Thermodynamics*, Cambridge Univ. Press, New York.

O'Gorman, P. A. (2012), Sensitivity of tropical precipitation extremes to climate change, *Nat. Geosci.*, *5*, 697–700, doi:10.1038/ngeo1568.

O'Gorman, P. A., and T. Schneider (2009), The physical basis for increases in precipitation extremes in simulations of 21st century climate, *Proc. Natl. Acad. Sci. U.S.A.*, *106*, 14,773–14,777.

Shaw, S. B., A. A. Royem, and S. J. Riha (2011), The relationship between extreme hourly precipitation and surface temperature in different hydroclimatic regions of the United States, *J. Hydrometeorol.*, *12*(2), 319–325.

Sugiyama, M., and H. Shiogama (2010), Precipitation extreme changes exceeding moisture content increases in MIROC and IPCC climate models, *Proc. Natl. Acad. Sci. U.S.A.*, *107*, 571–575, doi:10.1073/pnas.0903186107.

Thompson, R. L., R. Edwards, J. A. Hart, K. L. Elmore, and P. Markowski (2003), Close proximity soundings within supercell environments obtained from the rapid update cycle, *Weather Forecasting*, *18*, 1243–1261, doi:10.1175/1520-0434(2003)018<1243:CPSWSE>2.0.CO;2.

Trenberth, K. (1999), Conceptual framework for changes of extremes of the hydrological cycle with climate change, *Clim. Change*, *42*(1), 327–339.

Trenberth, K. (2011), Changes in precipitation with climate change, *Clim. Res.*, *47*, 123–138, doi:10.3354/cr00953.

Utsumi, N., S. Seto, S. Kanae, E. E. Maeda, and T. Oki (2011), Does higher surface temperature intensify extreme precipitation?, *Geophys. Res. Lett.*, *38*, L16708, doi:10.1029/2011GL048426.

Wallace, J. M. (1975), Diurnal variations in precipitation and thunderstorm frequency over the conterminous United States, *Mon. Weather Rev.*, *103*, 406–419.

Ye, B., A. D. Del Genio, and K. K.-W. Lo (2010), CAPE variations in the current climate and in a climate change, *J. Clim.*, doi:10.1175/1520-0442(1998)011<1997:CVITHCC>2.0.CO;2.